LONGITUDINAL RESPONSE MATRIX SIMULATIONS FOR THE SWISSFEL INJECTOR TEST FACILITY

A. Saa Hernandez*, B. Beutner†, F. Frei, R. Ischebeck, PSI, Villigen, Switzerland

Abstract

The Singular Value Decomposition (SVD) method has been applied to the SwissFEL Injector Test Facility to identify and better expose the various relationships among the possible jitter sources affecting the longitudinal phase space distribution and the longitudinal diagnostic elements that measure them. To this end, several longitudinal tracking simulations have been run using the Litrack code. In these simulations the RF and laser jitter sources are varied one-by-one within a range spanning several times their measured stability. The particle distributions have been dumped close to the diagnostic locations and the measured quantities analyzed. A matrix has been built by linearly fitting the response of each measured quantity to each jitter source. This response matrix is normalized to the stability of the jitter source and the instrumentation accuracy, and it is inverted and analyzed using SVD. From the eigenvalues and eigenvectors the sensitivity of the diagnostics to the jitters can be evaluated.

INTRODUCTION

The SwissFEL free electron laser [1] is currently being constructed at the Paul Scherrer Institute. The SwissFEL Injector Test Facility (SITF) has been operated since 2010 as a platform to develop and test the different components and optimize the procedures necessary to operate later SwissFEL.

Several sources of jitter and drift affect the longitudinal phase space dynamics of the SITF. In order to identify and better expose the various relationships among the error sources and the longitudinal diagnostics that measure them, longitudinal response matrix simulations have been performed for the SITF in a similar manner as previously realized for SwissFEL [2]. These simulations have been used to predict the response matrix later measured at SITF during two shifts. A detailed description and analysis of the experimental results is given on a separate contribution [3].

A scheme of the SITF showing the longitudinally relevant elements is sketched in Figure 1. The electrons emerge from an S-band RF photoinjector and are accelerated by a booster linac based on normal conducting S-band RF technology, which simultaneously generates the necessary energy chirp for the magnetic compression. In front of the magnetic chicane a fourth harmonic X-band cavity, phased for deceleration, linearizes the longitudinal phase space for optimal bunch compression. The last drift section is dedicated to the beam characterisation.

The bunch charge is measured with stripline beam position monitors (BPM), that were calibrated via a Faraday cup and a wall-current monitor [4]. BPMs in dispersive sections measure the horizontal beam position from which the mean particle energy is inferred, while the energy distribution is measured by imaging the incoherent synchrotron radiation with a monitor (SRM) [5]. The bunch arrival time monitor (BAM) samples the deviation of a RF pick-up signal from the electron bunch with a pulsed reference laser [6]. The absolute bunch length is measured in a destructive manner using a transverse deflective cavity (TDC) and imaging the bunch at a screen, while the relative bunch length variations are measured with a bunch compression monitor (BCM) based on coherent diffraction radiation (CDR) generated as the electron bunch passes through a hole in a foil. After passing through THz filters, the emitted CDR is detected by Schottky diodes [3]. An overview of the longitudinal diagnostics relevant for the response matrix studies is also shown in Figure 1.

SIMULATIONS

To analyze the sensitivity of the electron beam to RF-phase, RF-amplitude, and charge errors the entire beamline must be considered. The beamline is modeled in *LiTrack* [7], a one-dimensional tracking code which includes the effect of longitudinal wakefields. The physics model of Litrack is more appropriate for highly-relativistic beams. For this reason the following trick is applied to study the entire beamline; initially a low-energy high space-charge 3D tracking simulation is done with *Astra* [8] and a particle distribution at 130 MeV (after FINSB02) is generated. The energy and longitudinal coordinates of these particles are used as a 1D input distribution for the LiTrack simulation, where it is firstly tracked backwards to the photocathode and afterwards tracked forward including the error sources. A total of 11 error sources have been studied in this work; the phase and amplitude of the photoinjector RF gun (ϕ_{SS}, A_{SS}), the phase and amplitude of the three S-band accelerating cavities (ϕ_{S1}, A_{S1}, ϕ_{S2}, A_{S2}, ϕ_{S3}, A_{S3}), the phase and amplitude of the linearizer X-band cavity (ϕ_X, A_X) and bunch charge (Q) due to laser fluctuations. The nominal settings of the charge and RF parameters in the simulations, presented in Table 1, are taken such to match those of the experiments performed at SITF. Thus, bunches of 20 pC are accelerated to a final energy of 200 MeV and compressed approximately 7 times their original length, from 1.9 ps (570 μm) down to 266 fs (79 μm) in the experiment, and only down to 85 μm, approximately 10% less compression, in the simulations with the same RF settings.

The tracking simulations are run varying the error sources one by one, in five steps, within the range shown in Table 1.

* angela.saa-hernandez@psi.ch
† presently at DESY, Hamburg

ISBN 978-3-95450-133-5

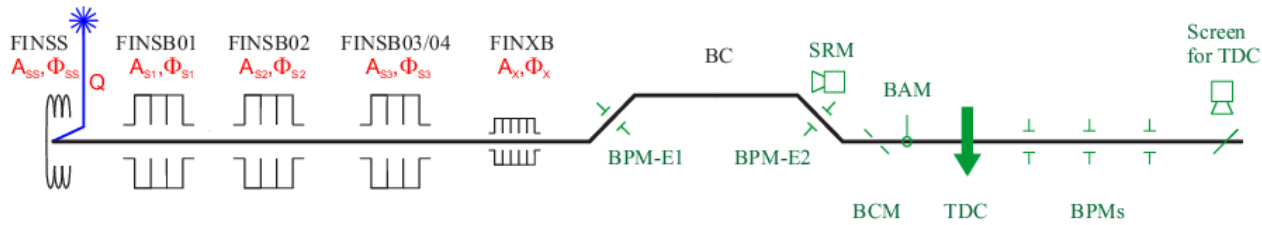

Figure 1: Scheme of the SwissFEL Injector Test Facility. In green the longitudinal diagnostics sketched at their positions, in red the error sources studied in this work.

Table 1: Initial settings and variation range of the longitudinal error sources that match the experimental conditions. The stability was measured during the experiments.

Parameter	Settings	Variation Range	Stability
ϕ_{SS}	4.3 °	± 1.5 °	0.039 °
A_{SS}	7.02 MV	± 7.4 %	0.041 %
ϕ_{S1}	-0.02 °	± 1.5 °	0.022 °
A_{S1}	53.57 MV	± 1.7 %	0.011 %
ϕ_{S2}	-2.5 °	± 1.5 °	0.026 °
A_{S2}	70.80 MV	± 0.5 %	0.007 %
ϕ_{S3}	-37.5 °	± 1.5 °	0.035 °
A_{S3}	102.65 MV	± 6.0 %	0.056 %
ϕ_X	180.04 °	± 1.5 °	0.18 °
A_X	14.21 MV	± 8.6 %	0.13 %
Q	20 pC	± 9 %	0.9 %

This range was defined experimentally. An example of the particle distribution tracked along the beamline for the five steps of the ϕ_{S3} variation range is shown in figure 2. The particle distribution is projected along the longitudinal position axis and the energy axis. The variation in arrival time and bunch compression is clearly visible for the different steps.

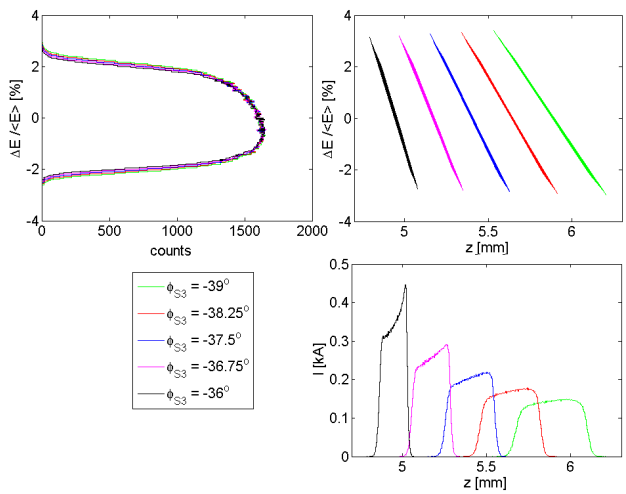

Figure 2: Particle distribution tracked with Litrack along the entire beamline, for the five steps variation of ϕ_{S3}.

The particle distributions are dumped close to the diagnostic locations and analyzed such to extract the parameter that would be measured by each diagnostic element. In this manner, most of the diagnostic elements are not yet modeled in this first approximation to the response matrix problem. Thus, to get the energy at the position of the SRM and of the BPMs in the bunch compressor (BPM-E1, BPM-E2) the energy outputs provided by the LiTrack code close to those positions are simply taken. Similarly, to get the charge from the stripline BPMs the charge output of the LiTrack code after the bunch compressor is taken. To get the bunch length at the screen which images the bunch deflected by the TDC the particle distribution is projected along the longitudinal position axis and the rms is taken. Similarly, for the energy spread measurements at the SRM the rms from the particle distribution projected along the energy axis is taken. The BCM is the only diagnostic element which had to be modeled in order to be able to extract from the particle distribution the parameter it measures. To get the relative bunch length variations the current profile was generated from the projection of the particle distribution along the longitudinal position axis. From this, the power spectrum was derived and subsequently multiplied by the single electron spectrum and the spectral responsivity of the detectors used. The single electron spectrum was simulated by the numerical code *THz Transport* [9], taking into account the experimental geometry. For the two BCMs, the CDR is thereafter integrated in two spectral bands (BCM-D1r: 0.6 – 2 THz, BCM-D2r: 0.26 – 2 THz). The cut-on frequency of the high pass THz filter determines the sensitivity of the BCM.

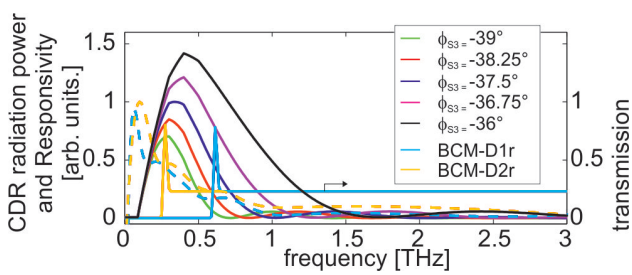

Figure 3: CDR radiation power corresponding to the ϕ_{S3} phase variation range and transmission of the THz filters and the spectral responsivities of the corresponding detectors (blue and yellow).

An example of the CDR generated for the five steps of the ϕ_{S3} variation range is shown in Figure 3. All the diagnostics elements, the corresponding measured parameters and

ISBN 978-3-95450-133-5

Table 2: Longitudinal Diagnostics and Their Resolution

Diagnostics	Quantity measured	Resolution
BPM-E_1	energy	0.013 MeV
SRM-E	energy	0.024 MeV
SRM-ΔE	energy spread	0.024 MeV
BPM-E_2	energy	0.013 MeV
BCM-D1r	CDR, integr. 0.6–2 THz	1.6 mV (0.8 %)
BCM-D2r	CDR, integr. 0.26–2 THz	2.4 mV (0.6 %)
BPM-Q	charge	0.062 pC (0.3 %)
BAM-t	bunch arrival time	52 fs
TDC-σ_z	bunch length	40 fs

its resolution, estimated experimentally, are presented in Table 2.

The quantities measured by the diagnostics are plotted for the error variation range. The response of the diagnostic to the error is defined by the slope of the linear fit. An example of the ϕ_{S3} variation measured by the 9 available diagnostic elements is shown in Figure 4.

The same is done for each of the 11 error sources, such that a 11×9 response matrix is obtained. To convert it into a dimensionless matrix where the terms can be compared, the responses are multiplied by the stability of the error sources and divided by the diagnostic resolution, shown in Tables 1 and 2, respectively. The resulting dimensionless response matrix is presented in Table 3. It can be observed that while the charge measurement using BPM-Q is only sensitive to the charge variation, all other diagnostics are sensitive to a combination of error sources.

Thus, in order to analyze the response matrix R the SVD method has been used. For this purpose R is decomposed into three matrices according to:

$$R = U \cdot \Sigma \cdot V^T \tag{1}$$

where the matrix Σ, presented in Table 4, contains the square roots of the singular values ordered from greatest to least along its diagonal. With the aim to account for the most significant correlations, we have restricted Σ to the first five singular values, and neglected the remaining ones. In order for the matrix multiplication to be consistent we have eliminated the corresponding column vectors of U and V. From the resulting matrices U and V with reduced dimensionality, shown in Tables 5 and 6, we can observe:

- The first singular value indicates a mode acting mainly on the bunch compression, which relates the variations of ϕ_{S3} and ϕ_X with the measurements from BCM-D1r and BCM-D2r. It is worth emphasizing that for the simulations the bunch length was roughly 10% longer and the bunch shape showed steeper rising and falling edges than the profile measured during the experiments. These deviations affect the resolution of the BCM, and since the resolution from the experimental measurement is used for normalization, this leads to an increase of the sensitivity of the BCM in the present simulations.
- The second singular value indicates a mode acting on the mean energy of the particles. The diagnostics BPM-E_1, BPM-E_2 and SRM-E measure energy changes caused mainly by variations of the phases ϕ_{S3} and ϕ_X and the amplitudes A_{S3} and A_X.
- The third singular value indicates a mode acting on the charge, which is measured by BPM-Q and in a smaller scale by the BCM monitors that measure variations of the bunch charge.
- The fourth singular value, almost 10^3 times smaller than the first one, indicates a combined mode acting on energy spread, bunch compression and charge, caused by the phase and amplitude of FINSB03 (ϕ_{S3} and A_{S3}) and the phase and amplitude of FINXB (ϕ_X and A_X).
- The fifth singular value is already so small, more than 10^5 times smaller than the first singular value, that is just dominated by noise and has no constructive impact on the response matrix.

CONCLUSIONS

A diagnostics response matrix for the SwissFEL Injector Test Facility has been simulated and afterwards experimentally measured. The simulation work used to predict the measurement results has been presented here. Because this simulation work does not yet include modeling of the different diagnostics including the detector responses, no quantitative comparison is yet to be done between the simulated and experimental response matrices. Still, the predicted sensitivities of some diagnostics to certain error sources and also the coupling between them have been later experimentally confirmed.

ACKNOWLEDGEMENTS

Initial particle distributions for the simulations in Litrack were provided by Simona Bettoni.

REFERENCES

[1] R. Ganter (ed.) “SwissFEL Conceptual Design Report”, PSI Bericht, 10-04, 2010.

[2] R. Ischebeck et al., “Response Matrix of Longitudinal Instrumentation in SwissFEL”, in Proc. 33rd Int. Free-Electron Laser Conf., Shanghai, 2011, pp. 652-655.

[3] F. Frei et al., “Experimental Results of Diagnostics Response for Longitudinal Phase Space”, in These Proceedings: Proc. 36th Int. Free-Electron Laser Conf., Basel, 2014, THB02.

[4] B. Keil et al., “Commissioning of the Resonant Stripline BPM System of the SwissFEL Test Injector”, in Proc. 32nd Int. Free-Electron Laser Conf., Malmö, 2010, pp. 429-432.

[5] G.L. Orlandi et al., “Characterization of Compressed Bunches in the SwissFEL Injector Test Facility”, in Proc. Int. Beam Instrumentation Conf., Oxford, 2013, pp. 515-518.

[6] V. Arsov et al., “Commissioning and Results from the Bunch Arrival-time Monitor Downstream the Bunch Compressor at the SwissFEL Test Injector”, in These Proceedings: Proc. 36th Int. Free-Electron Laser Conf., Basel, 2014, THP085.

ISBN 978-3-95450-133-5

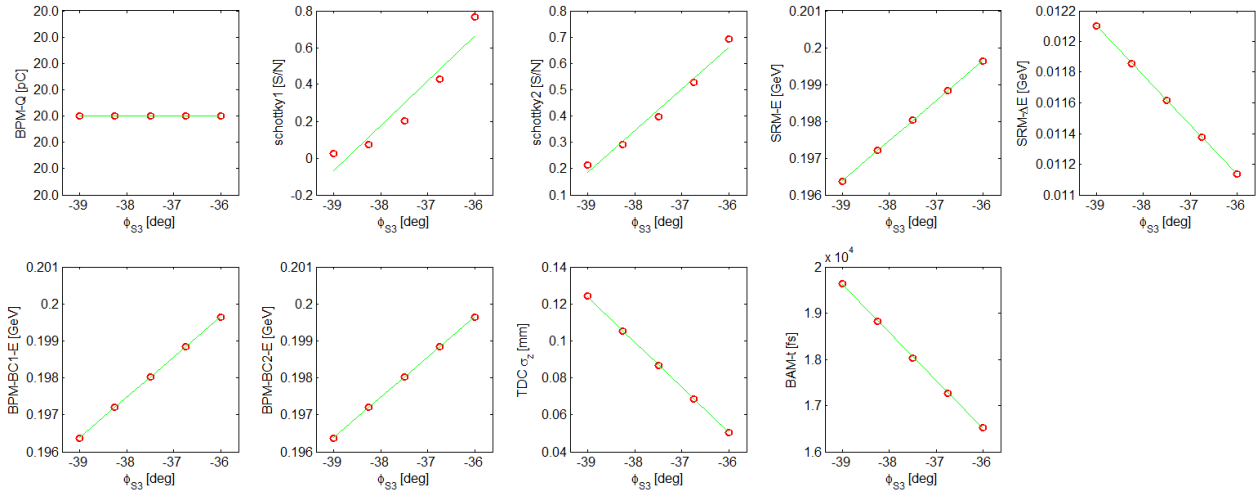

Figure 4: Variation of the ϕ_{S3} in five steps measured by each of the diagnostic measurements. A linear fit gives the response of the different diagnostics to this RF actuator.

Table 3: Response Matrix of the Diagnostics to the RF Variation (Matrix R).

	Q	ϕ_{SS}	ϕ_{S1}	ϕ_{S2}	ϕ_{S3}	ϕ_X	A_{SS}	A_{S1}	A_{S2}	A_{S3}	A_X
BPM-E_1	-0.01	-0.03	0	0.10	**2.75**	0	0.20	0.46	0.35	**3.26**	**-1.31**
SRM-E	-0.01	-0.01	0	0.06	**1.60**	0	0.12	0.27	0.21	**1.90**	-0.76
SRM-ΔE	-0.02	-0.04	-0.16	-0.24	-0.47	**1.34**	-0.01	-0.02	-0.01	0.15	0.05
BPM-E_2	-0.01	-0.03	0	0.10	**2.75**	0	0.20	0.46	0.35	**3.26**	**-1.31**
BCM-D1r	**2.41**	0.28	**1.29**	**2.07**	**5.39**	**-11.09**	0.17	0.36	0.26	0.37	-0.98
BCM-D2r	**3.07**	0.12	0.57	0.92	**2.36**	**-4.90**	0.08	0.16	0.12	0.16	-0.44
BPM-Q	**3.00**	0	0	0	0	0	0	0	0	0	0
BAM-t	0	0.01	0	-0.03	-0.73	0	-0.05	-0.12	-0.09	-0.87	0.35
TDC-σ_z	0	0	-0.02	-0.03	-0.07	0.15	0	0	0	-0.01	0.01

Table 4: Matrix Σ

	1	2	3	4	5
1	**14.52**	0	0	0	0
2	0	**6.59**	0	0	0
3	0	0	**3.41**	0	0
4	0	0	0	**0.02**	0
5	0	0	0	0	0.001

Table 5: Matrix U

	1	2	3	4	5
BPM-E_1	0.12	**0.63**	0.04	-0.02	-0.03
SRM-E	0.07	**0.37**	0.02	-0.01	-0.02
SRM-ΔE	-0.10	0.05	0.11	**0.60**	0.77
BPM-E_2	0.12	**0.63**	0.04	-0.02	-0.03
BCM-D1r	**0.88**	-0.14	**-0.26**	**0.35**	-0.11
BCM-D2r	**0.42**	-0.10	**0.45**	**-0.62**	0.47
BPM-Q	0.05	-0.06	**0.85**	**0.36**	-0.39
BAM-t	-0.03	-0.17	-0.01	0	-0.12
TDC-σ_z	-0.01	0	0.01	0.06	0.06

Table 6: Matrix V

	1	2	3	4	5
Q	0.25	-0.13	**0.96**	0	0
ϕ_{SS}	0.02	-0.01	-0.01	-0.02	0.08
ϕ_{S1}	0.10	-0.04	-0.03	-0.12	0.23
ϕ_{S2}	0.16	-0.04	-0.04	-0.17	0.02
ϕ_{S3}	**0.45**	**0.48**	-0.05	**0.66**	-0.31
ϕ_X	**-0.82**	**0.33**	0.26	**0.20**	-0.15
A_{SS}	0.02	0.04	0	-0.04	0.11
A_{S1}	0.04	0.10	0	-0.08	0.22
A_{S2}	0.03	0.07	0	-0.06	0.17
A_{S3}	0.09	**0.74**	0.08	**-0.28**	0.49
A_X	-0.10	**-0.27**	-0.01	**0.63**	0.70

[7] K.L.F. Bane and P. Emma, "Litrack: A Fast Longitudinal Phase Space Tracking Code with Graphical User Interface", in Proc. 2005 Particle Accelerator Conf., Knoxville, 2005, pp. 4266-4268.

[8] K. Flötmann, "ASTRA A Space Charge Tracking Algorithm", user manual available at: `http://www.desy.de/~mpyflo/Astradokumentation/`

[9] THz Transport, developed by B. Schmidt, DESY.

ISBN 978-3-95450-133-5